Geoscience Frontiers 11 (2020) 1069–1080

Contents lists available at ScienceDirect

Geoscience Frontiers

journal homepage: www.elsevier.com/locate/gsf

Research Paper

Cenozoic reactivation along the Late Triassic Ganzi-Litang suture, eastern Tibetan Plateau

W.T. Jackson Jr. [a,b,*], D.M. Robinson [b], A.L. Weislogel [c], X. Jian [d]

[a] Department of Earth Sciences, University of South Alabama, Mobile, AL, 36688, USA
[b] Department of Geological Sciences and Center for Sedimentary Basin Studies, The University of Alabama, Tuscaloosa, AL, 35487, USA
[c] Department of Geography and Geology, West Virginia University, Morgantown, WV, 26506, USA
[d] State Key Laboratory of Marine Environmental Science, College of Ocean and Earth Sciences, Xiamen University, Xiamen 361102, China

ARTICLE INFO

Handling Editor: Sanghoon Kwon

Keywords:
Nonmarine strata
Yidun terrane
Tibetan plateau
Zircon
Suture zone
Reactivation

ABSTRACT

The spatial-temporal development of Cenozoic reactivation along Mesozoic suture zones in the Tibetan Plateau are first-order parameters needed for assessing models of plateau growth. The Ganzi-Litang suture, in the eastern Tibetan Plateau, developed in the Late Triassic because of subduction and closure along the eastern branch of the Paleo-Tethys Ocean. Near the city of Litang, the Ganzi-Litang suture is defined by a mélange sequence with fault-bound, synorogenic nonmarine strata along the western and eastern flanks, suggesting post-Triassic structural reactivation. We present detrital zircon U–Pb geochronology and field data to determine the timing and style of reactivation along the Ganzi-Litang suture, as well as sedimentary provenance of nonmarine strata.

A reverse fault placing mélange rock on top of nonmarine strata along the eastern flank of the Ganzi-Litang suture indicates a contractional deformational regime during reactivation. Conglomerate clast counts indicate a local sediment source of recycled Ganzi-Litang suture and Yidun terrane rock. Detrital zircons indicate a localized provenance consisting of recycled material from Triassic Yidun Arc plutons and Triassic Yidun Group turbidite rock. A weighted mean average of Cenozoic zircon grains ($n = 10$) establishes a maximum depositional age of 41.5 ± 1.2 Ma for nonmarine strata in the Ganzi-Litang suture. We interpret the maximum depositional age of the nonmarine strata to represent the upper-limit for structural reactivation along the Ganzi-Litang suture while undeformed Neogene strata in the suture zone represent the lower-limit; thereby bracketing structural reactivation from ca. 42–25 Ma. Our results provide enhanced spatial-temporal resolution for Cenozoic deformation in the eastern Tibetan Plateau.

1. Introduction

Suture zones, defined by ophiolite and mélange rock, are located in the interior Tibetan Plateau and mark sites of oceanic lithosphere destruction resulting from Mesozoic terrane collisions (e.g., Dewey, 1977; Dewey et al., 1988; Yin and Harrison, 2000; Zhang et al., 2012). Reactivation along pre-existing sutures is a fundamental feature of lithospheric deformation that governs many tectonic processes within orogenic systems and rifted margins (Thomas, 1977; Daly et al., 1989; Molnar, 1989; Marshak et al., 2000). Because of the lack of lithospheric strength in the pre-existing sutures, far-field forces cause sutures to preferentially host and re-host deformation, which is expressed through complex displacement, internals strain, and crustal block rotations (e.g., Dewey and Burke, 1973; Thatcher, 1995; Holdsworth et al., 1997, 2001; Marshak et al., 2000; Tapponnier et al., 2001). Understanding the tectonic history for these lithospheric zones of weakness remains a first-order requirement for advancing models of modern and ancient orogenic systems.

Reconstruction of suture zones often proves difficult, fortunately sedimentary strata preserved in and adjacent to these complex regions provide records of their tectonic development (e.g., Ridgway et al., 2002; Kapp et al., 2007; Orme et al., 2015; Leary et al., 2016). Deformation associated with the reactivation of pre-existing Mesozoic suture zones throughout the Tibetan Plateau is recorded by nonmarine deposition (Yin and Harrison, 2000; Tapponnier et al., 2001; Horton et al., 2002, 2004; Leier et al., 2007a,b; Staisch et al., 2014). Nonmarine strata

* Corresponding author. Department of Earth Sciences, University of South Alabama, Mobile, AL, 36688, USA.
E-mail address: wjackson@southalabama.edu (W.T. Jackson).
Peer-review under responsibility of China University of Geosciences (Beijing).

https://doi.org/10.1016/j.gsf.2019.11.001
Received 19 February 2019; Received in revised form 3 September 2019; Accepted 3 November 2019
Available online 23 November 2019

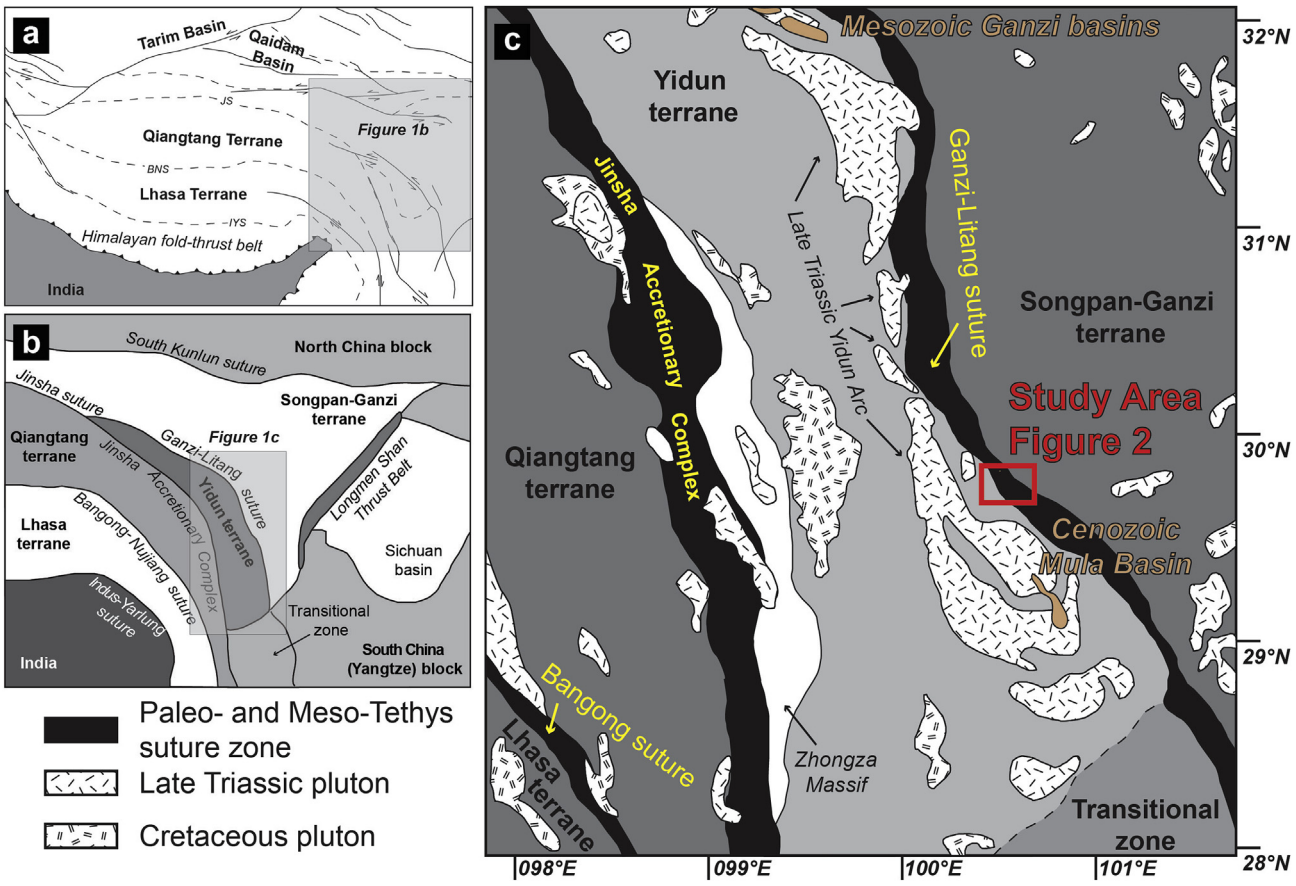

Fig. 1. (a) Map of the Tibetan Plateau region, illustrating the terranes and suture zones. JS–Jinsha-Jiang suture, IYS–Indus-Yarlong suture, BNS–Bangong-Nijiang suture. (b) Tectonic map from the eastern Tibetan Plateau. (c) Generalized tectonic map for the Yidun terrane, highlighting the spatial relationship of the Ganzi-Litang suture, the Late Triassic Yidun Arc, the Cenozoic Mula Basin, the Mesozoic Ganzi basins, and the study area.

unconformably overlie Mesozoic rock and tend to be structurally located in the footwalls of thrust faults (Spurlin et al., 2005; Studnicki-Gizbert et al., 2008). Jackson et al. (2018a, b) documented contrasting age determinations of Late Cretaceous and Oligocene–Miocene for nonmarine strata in the Yidun terrane, highlighting the need for better temporal resolution of nonmarine deposits in the eastern Tibetan Plateau.

The Yidun terrane, positioned between the eastern Himalayan syntaxis and the Xianshuihe fault system, hosts numerous nonmarine basins that present an opportunity to understand the regional tectonic development (Wang and Burchfiel, 2000; Burchfiel and Chen, 2012). The eastern margin of the Yidun terrane is defined by a mélange sequence that defines the Late Triassic Ganzi-Litang suture (Fig. 1). The Ganzi-Litang suture also contains fault-bounded, nonmarine strata along the structural flanks of the suture, suggesting post-Triassic reactivation. We present detrital zircon U–Pb geochronology and field data from the Ganzi-Litang suture (Fig. 1) to explore the structural style of deformation, timing of reactivation, and the sedimentary provenance of nonmarine strata. The objectives of this study are to advance our understanding of the tectonic development of the Ganzi-Litang suture and the spatial-temporal relationship of nonmarine deposition in the eastern Tibetan Plateau.

2. Geologic setting

The Ganzi-Litang suture is ~600 km in length and marks the boundary between the Yidun and Songpan-Ganzi terranes (Fig. 1c). To the northwest, the Ganzi-Litang suture merges with the Jinsha-Jiang suture. Based on structural field measurements, the age of pluton emplacement, and pluton geochemical signatures, the Ganzi-Litang suture and Jinsha-Jiang suture are interpreted to be a correlative, continuous tectonic element throughout the interior portions of the eastern and central parts of the plateau (Reid et al., 2005; Yang et al., 2012). The termination of the Ganzi-Litang suture to the southeast is less defined, as it dissipates into the transitional zone between the Yangtze block (South China) and Qiangtang terrane (Burchfiel and Chen, 2012).

The age of Yidun Arc plutons, which crop out in the eastern part of the Yidun terrane west of the Ganzi-Litang suture, provide the primary indicator for the timing of suture development (Weislogel, 2008). Yidun Arc plutons are Late Triassic (215–224 Ma), calc-alkaline, I-type granites that regionally intrude deformed Triassic Yidun Group turbidite sequences (Reid et al., 2007; Weislogel, 2008; Leng et al., 2014; Peng et al., 2014). The spatial distribution and geochemistry of the Yidun Arc suggest that the emplacement of the plutons resulted from westward subduction of the Songpan-Ganzi terrane beneath the eastern Yidun terrane (Hou, 1993; Reid et al., 2007; Weislogel, 2008; Peng et al., 2014). Wang et al. (2013) used detrital zircon U–Pb geochronology of the Triassic Yidun Group turbidite rock to suggest that the Ganzi-Litang suture developed first in the southeastern part of the Yidun terrane and progressed northwestward from ca. 230–220 Ma. However, Jian et al. (2019) suggested that the similarity of detrital zircon U–Pb ages in Middle–Late Triassic turbidite rock in the Songpan-Ganzi and Yidun terranes indicates that the closure of the Ganzi-Litang suture occurred during the Middle Triassic. Li et al. (2017) reported retrograde metamorphism at 218 Ma for garnet amphibolite facies within the Ganzi-Litang suture using in-situ U–Pb sphene, supporting a Late Triassic age for development of the GLS.

Near Litang, the Ganzi-Litang suture is an ~5 km wide mélange rock sequence, consisting of units from west to east of Triassic Yidun Group

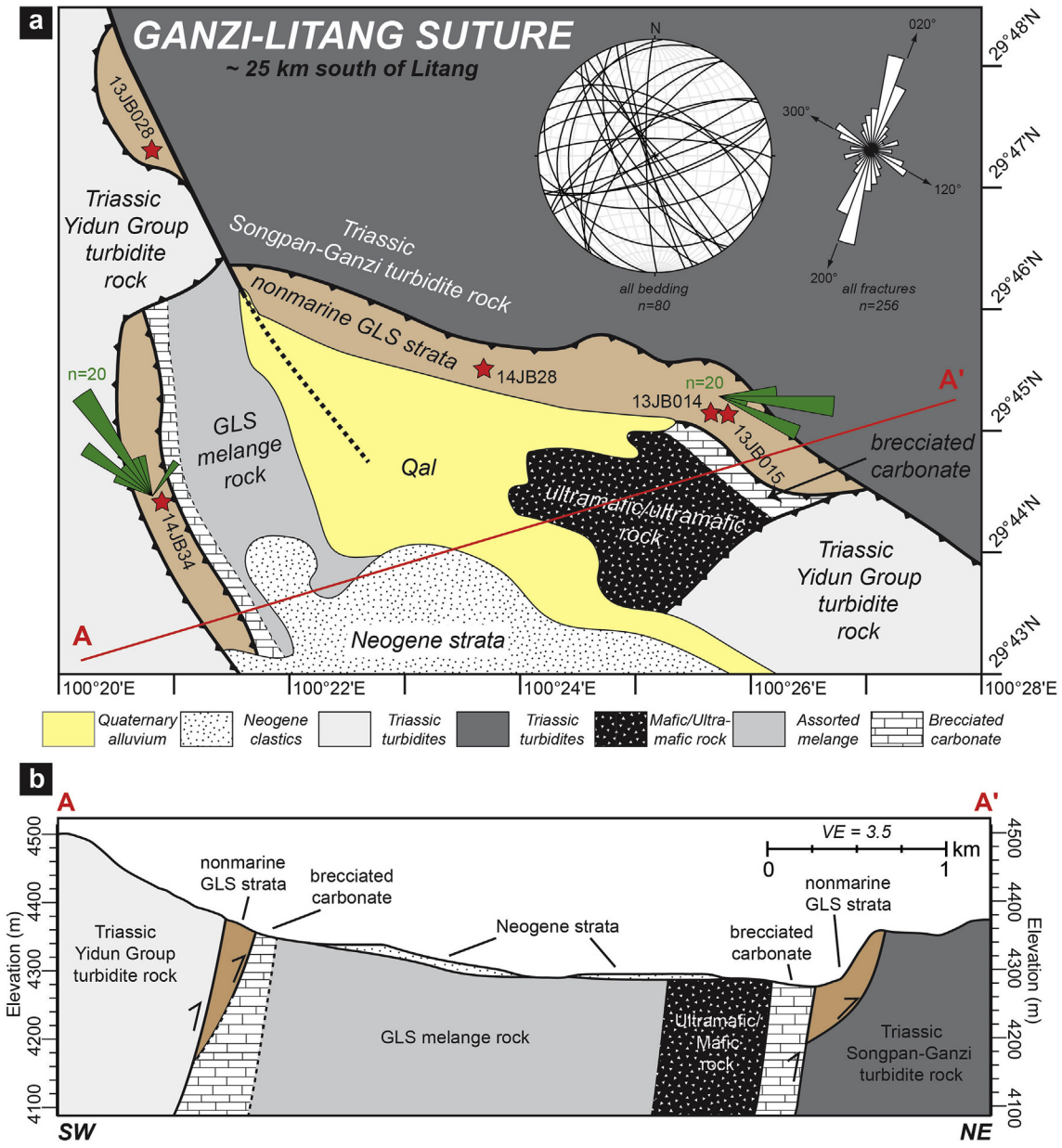

Fig. 2. (a) Geologic map and corresponding (b) schematic cross section of the Ganzi-Litang suture approximately 25 km south of Litang in southwestern Sichuan Province, China. Structural bedding (taken from all units) and fracture (only recorded in the nonmarine strata unit) measurements displayed in upper-right corner through steronet and rose diagram projections. Green rose diagram bars illustrate direction of measured clast imbrications in conglomerate interbeds, indicating paleoflow direction. Red stars show location of samples collected for detrital zircon U–Pb geochronology. Topographic profile for cross section created from GEOMAP App.

turbidite rock, nonmarine interbedded conglomerate, sandstone, and mudstone, brecciated limestone, garnet amphibolite, ultra-mafic peridotite, brecciated limestone, nonmarine interbedded conglomerate, sandstone, and mudstone, and Songpan-Ganzi turbidite rock (Figs. 2 and 3). Subhorizontal, undeformed Neogene strata unconformably overlies Ganzi-Litang suture mélange rock, ranging in thicknesses from 5 m to 12 m (Figs. 2b and 3a).

3. Methods

3.1. Field data

Investigation of the Ganzi-Litang suture was conducted during three field seasons in 2013 and 2014. Rock samples were collected for detrital zircon U–Pb geochronology analysis. Sampling distribution and density were controlled primarily by rock type and accessibility. Conglomerate clast counts, bedding and fault orientations, and fracture measurements were collected to document sedimentological and structural relationships. For clast counts, the rock type of 50–100 clasts was identified using 2 cm spacing over an ~1 m grid. Detailed rock descriptions, field data, and sample locations are in Supplemental File S1.

3.2. Detrital zircon U–Pb geochronology

Five samples from nonmarine strata were analyzed for detrital zircon U–Pb geochronology. One to 4 kg were collected from sandstone and granule conglomerate samples. Zircon grains were separated using a jaw crusher, disk mill, water table, magnetic (frantz) separator, and heavy (MEI) liquids at the University of Alabama. Unknown zircon grains, along with standard Sri Lanka (Kroner et al., 1987) and R33 (Black et al., 2004)

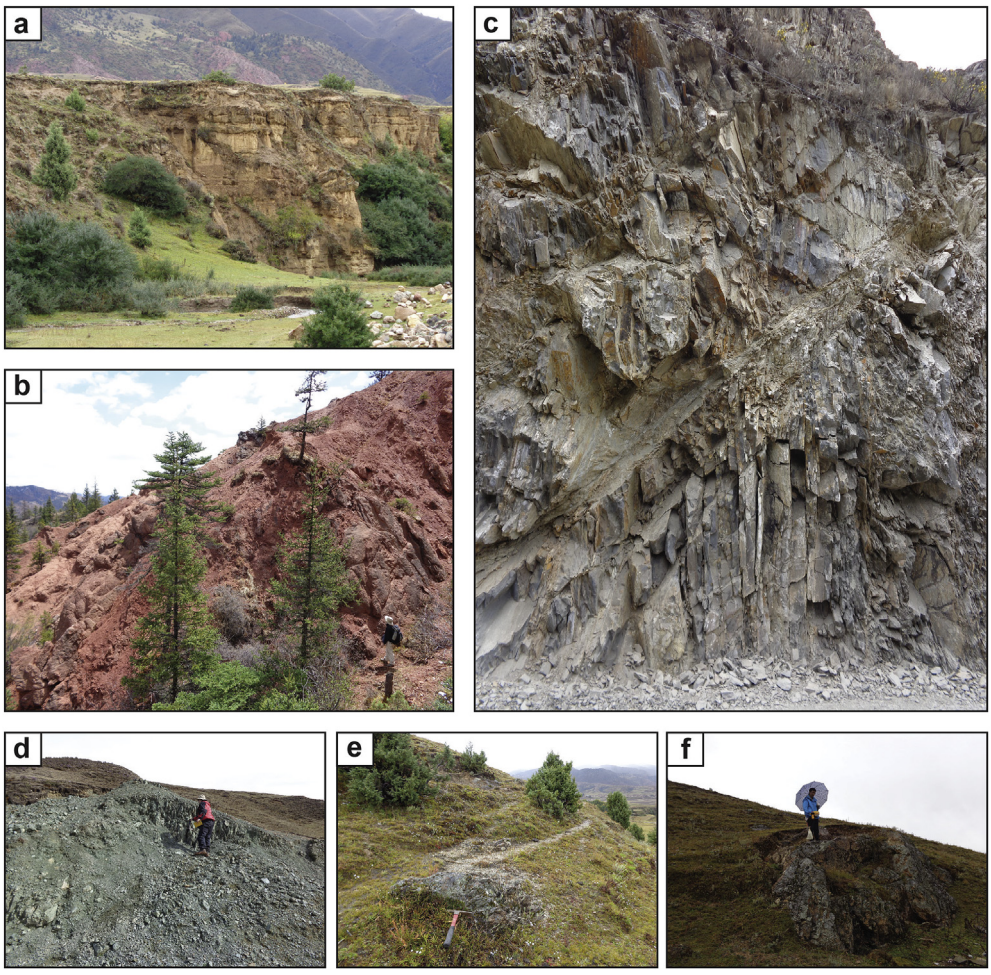

Fig. 3. Field photos from the Ganzi-Litang suture illustrating various rock units within, structurally juxtaposed, and stratigraphically overlying the suture's mélange sequence: (a) undeformed Neogene clastic strata, (b) nonmarine strata, (c) Late Triassic Yidun Group turbidite rock, (d) mafic/ultramafic unit, (e) amphiboblite schist unit, and (f) quartzite unit.

zircon fragments were mounted, abraded, polished, and imaged (back scatter electron) at the University of Arizona LaserChron Center (Gehrels et al., 2008; Gehrels and Pecha, 2014). Isotope values were collected with a Nu Plasma multi-collector LA-ICP-MS (samples 14JB34 and 13JB014) and an Element 2 single collector LA-ICP-MS (samples 13JB028, 13JB015, and 14JB28). Zircon data reduction (background, Hg, and fractionation corrections) were calculated in the excel software program Agecalc (Gehrels et al., 2008). Data are presented using routines produced in Isoplot (Ludwig, 2012) and DensityPlotter (Vermeesch, 2012). Detrital zircon U–Pb geochronology data are in Supplemental File S2.

4. Results and interpretations

4.1. Ganzi-Litang suture

Along the western flank of the Ganzi-Litang suture, an ~35–40 m thick sequence of nonmarine strata is fault-bound to the west by Yidun Group turbidite rock and to the east by GLS mélange rock. While a direct measurement of the bounding faults could not be obtained, based on structural measurements of bedding planes directly above and below, both bounding faults seem to be oriented ~155°, 67°SW. On the eastern flank of the Ganzi-Litang suture, nonmarine strata are bound to the northeast by Songpan-Ganzi turbidite rock and to the southwest by Ganzi-Litang suture mélange rock (Fig. 4). The southwestern bounding fault places brecciated carbonate rock above the nonmarine strata and is oriented 125°, 47°SW. The northeastern bounding fault is characterized by a fault zone with an overall reverse sense of motion and is oriented 255°, 75°SW (Fig. 4). A subsidiary normal fault, resulting from drag folding and slip, defines the fault contact with Songpan-Ganzi turbidite rock in the footwall and nonmarine strata in the hanging-wall (Fig. 4).

Because of the proximity (~25 km) of the strike-slip Litang fault to the study area and the reverse-sense of motion along the bounding faults in the Ganzi-Litang suture, the tectonic setting associated with the deposition of synorogenic nonmarine strata requires examination. The Litang fault is an active NW–SE trending, 190 km long and 25 km wide, left-lateral strike-slip fault that developed during Miocene time (Wang and Burchfiel, 2000; Zhang et al., 2015). The Litang fault is separated in an en echelon fashion into four, from NW to SE the Cuopu, Maoya, Litang, and South Jawa-Dewu segments (Chevalier et al., 2016). The development of the Litang fault corresponds temporally with other strike-slip faults such as the Xianshuihe fault to the north and the Red River fault zone to the south, which act together as a system to extrude crustal material southeastward (Royden et al., 2008; Burchfiel and Chen, 2012). Along the en echelon Litang and South Jawa-Dewu segments of the Litang fault extensonal releasing bends are developing, which negates the possibility that the bounding reverse-faults in the suture zone are associated with a restraining bend. One way to decipher between tectonic settings is the evaluation of fracture set orientations in a structural system (Engelder, 1987). Fracture data in nonmarine strata throughout the Ganzi-Litang suture exhibit a prominent ~NE–SW trend (i.e., Fig. 2a), indicating a sigma-one stress oriented perpendicular to the trend of the reverse faults. If fractures in the nonmarine strata developed in a

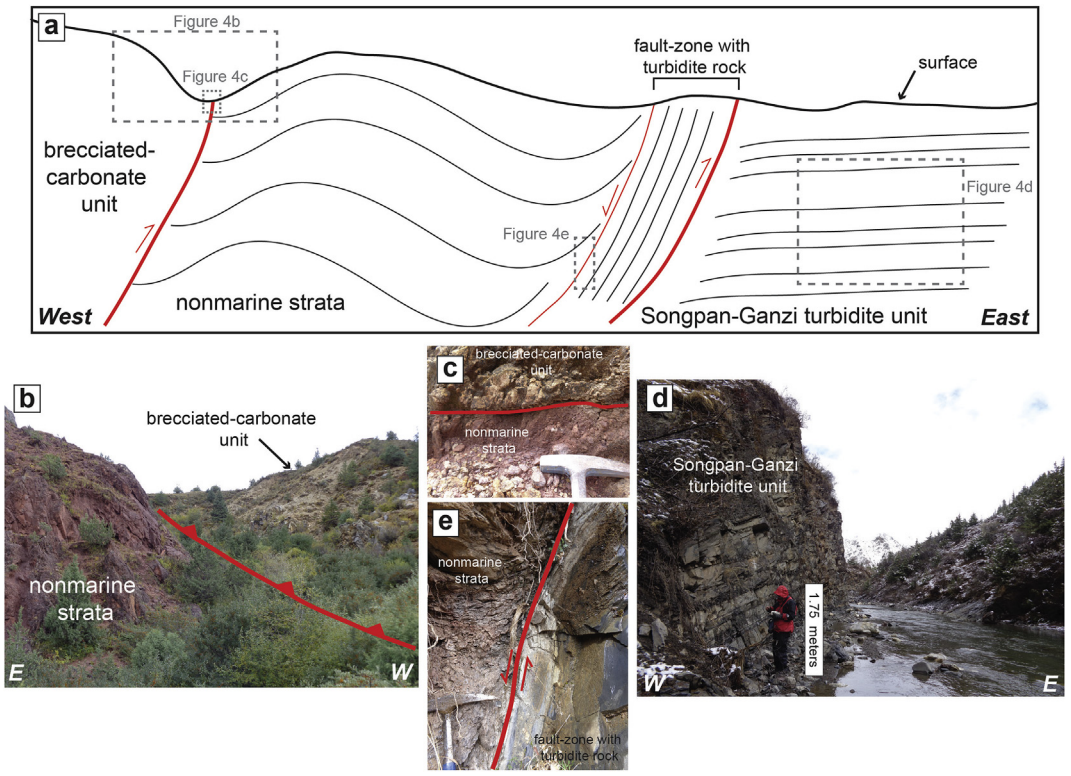

Fig. 4. Fault-bound nonmarine strata along the eastern flank of the Ganzi-Litang suture. Nonmarine strata are structurally juxtaposed to brecciated carbonate mélange rock to the west (b and c) and Triassic Songpan-Ganzi turbidite rock to the east (d and e).

strike-slip regime, fractures would usually exhibit an oblique orientation compared to the fault trend. Therefore, we interpret the deformation associated with nonmarine deposition in the Ganzi-Litang suture to be associated with a contractional tectonic regime that presumably pre-dated the Miocene strike-slip development of the Litang fault and other strike-slip systems in the eastern Tibetan Plateau.

4.2. Synorogenic nonmarine strata

Nonmarine Ganzi-Litang suture strata consists primarily of red and maroon conglomerate, with small (<1 m) interbeds of mudstone, siltstone, and sandstone. Conglomerate beds are clast-supported, with clasts ranging in size from 1 cm to 24 cm, exhibiting a biomodel size distribution with the majority of the clasts either 1–4 cm or 14–18 cm in diameter. Imbrications of the conglomerate clasts are locally present. Measured imbrications exhibit a wide range of paleoflow directions (Fig. 2a). Conglomerate clastrock types include sandstone (gray, tan, and red color), dark-gray to black shale/slate, schist, granite, ultra-mafic peridotite, meta-carbonate, quartzite, and quartz (Fig. 5). In total, 610 clasts were counted with the following occurrences: 19% sandstone, 21% shale/slate, 1% schist, 6% quartz, 17% granite, 12% ultra-mafic/mafic, 5% meta-carbonate, and 19% quartzite. Abundance of sandstone and shale clasts increase upsection, while mélange (metamorphic and ultra-mafic/mafic) and Yidun Arc (granite) derived clasts decrease upsection in nonmarine strata on both the western and eastern flanks. Ultramafic/mafic clasts are only present in conglomerate on the eastern flank.

We interpret an alluvial depositional environment for nonmarine strata in the Ganzi-Litang suture, based on clast compositions that indicate recycling of local Ganzi-Litang suture and Triassic turbidite rock, red to maroon color indicative of subaerial exposures, indentions on conglomerate clasts that suggest debris flow transport, and lack of bedding laminations. Because of the general lack of sandstone and mudstone interbeds throughout the nonmarine strata, we suggest that the GLS nonmarine strata may represent a proximal sub-environment(s) in the alluvial fan architecture.

4.3. Nonmarine strata provenance

Detrital zircon analysis of nonmarine Ganzi-Litang suture strata (n = 947) indicate age populations at 40–50 Ma (1%), 200–250 Ma (23%), 250–300 Ma (7%), 400–480 Ma (8%), 720–880 Ma (10%), 900–1000 Ma (6%), ~1800 Ma (19%), and ~2450 Ma (7%), with all other grains representing 19% occurrence (Fig. 6). The most abundant population, 200–250 Ma, correlates to Triassic Yidun Arc plutons, which show a biomodal ~218 Ma and ~238 Ma age distribution and are located to the east and proximal along the entire length of the Ganzi-Litang suture. Besides the Cenozoic 40–50 Ma population, all age Mesozoic and older age populations can be correlated to Triassic Yidun Group turbidite geochronology results (Weislogel et al., 2006, 2010; Ding et al., 2013; Wang et al., 2013a; Jian et al., 2019).

When nonmarine Ganzi-Litang suture strata zircon U–Pb geochronology are compared to other Mesozoic (west and east Ganzi basins) and Cenozoic (Mula basin) nonmarine sequences in the Yidun terrane, a correlation between the Cenozoic Mula basin exist through similar age populations (Fig. 7). This similarity is presumably a result of similar timing and spatial development between nonmarine Ganzi-Litang suture strata and the Mula basin. Both the nonmarine Ganzi-Litang suture strata and the Mula basin are located in the southeastern part of the Yidun terrane; whereas, the west and east Ganzi basins are located in the northeastern part of the Yidun terrane.

A source for detrital Eocene grains in the nonmarine strata remains elusive. In other regions throughout the plateau, the emplacement of Cenozoic magmatic bodies near Mesozoic sutures is accompanied by the development of nonmarine deposition (Roger et al., 2000; Chung et al., 2005; Wang et al., 2008a, b; Xia et al., 2011). Numerous plutonic bodies in the region match the U–Pb age of the Eocene grains; however, the closest pluton (Haizi) is ~100 km west of the Ganzi-Litang suture nonmarine strata. This distance is hard to integrate with a local sedimentary

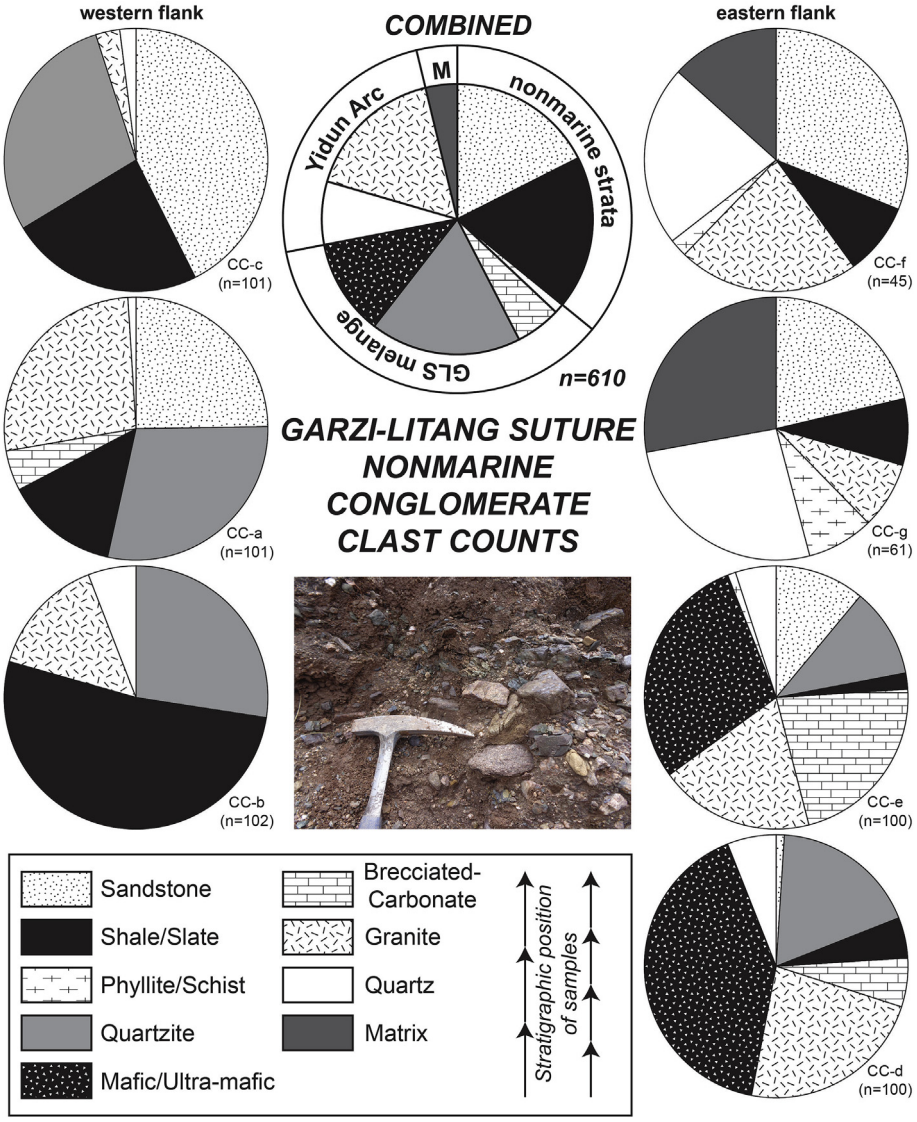

Fig. 5. Pie charts illustrating the modal occurences of various clast lithologies in conglomerate beds within the Ganzi-Litang suture's fault-bound nonmarine strata. Conglomerate clast counts have been organized based on geographic location (western and eastern flanks) and by stratigraphic position. Insert picture shows typical conglomerate outcrop exposure.

source interpretation. Possible sources for Eocene grains include aerial transport, removal of the proximal Cenozoic magmatic body/bodies because of erosion during uplift, and southeastward extrusion of the magmatic source. Below we briefly summarize the various hypotheses for the Eocene grains to highlight the need for future provenance examination.

Aerial transport of grains expelled during volcanism may have been transported significant distances, subsequently falling to the surface during nonmarine deposition. Pullen et al. (2011) provided an analogue example of detrital zircon transport via wind for the Chinese Loess Plateau, in which they show that detrital material was sourced aerially from the Qiadam Basin and northern Tibetan Plateau. We envision a sediment transport, deposition, and deformation relationship for the Eocene grains in the nonmarine Ganzi-Litang suture strata similar to that of DeCelles et al. (2007a,b) for synorogenic, aerially transported grains in northwestern Argentina.

Shallow emplacement of plutonic bodies and their associated surficial volcanics, proximal to the Ganzi-Litang suture, may have been erased from the rock record via erosion during regional exhumation. Late Cenozoic exhumation of the eastern Tibetan Plateau has promoted significant denudation of material in the region (e.g., Clark et al., 2005b). Therefore, the source for nonmarine Ganzi-litang suture Cenozoic grains may no longer be present in the rock record.

The source of Cenozoic grains in the nonmarine Ganzi-Litang suture strata may be located to the southeast between the eastern Himalaya syntaxis and the Ailao Shan shear zone. While the present tectonic configuration is hard to substantiate as a sediment source for nonmarine Ganzi-Litang suture strata, upon paleorestoration of southeastwardly extruded crustal material by strike-slip deformation, crustal blocks would have been more proximal to the Ganzi-Litang suture during early-middle Cenozoic time (e.g., LeLoup et al., 1995; Wang and Burchfiel, 1997; Tapponnier et al., 2001; Royden et al., 2008).

4.4. Age of nonmarine strata

Traditional indicators of stratigraphic age are absent in nonmarine Ganzi-Litang suture strata. Because these strata share similar sedimentological characteristics to other nonmarine stratigraphic successions in the Yidun terrane that exhibit both Late Oligocene–Early Miocene (Mula basin; Jackson et al., 2018a) and Late Cretaceous (Ganzi basins; Jackson et al., 2018b) ages, the age for nonmarine Ganzi-Litang suture strata requires examination. Since all five samples collected occur in close

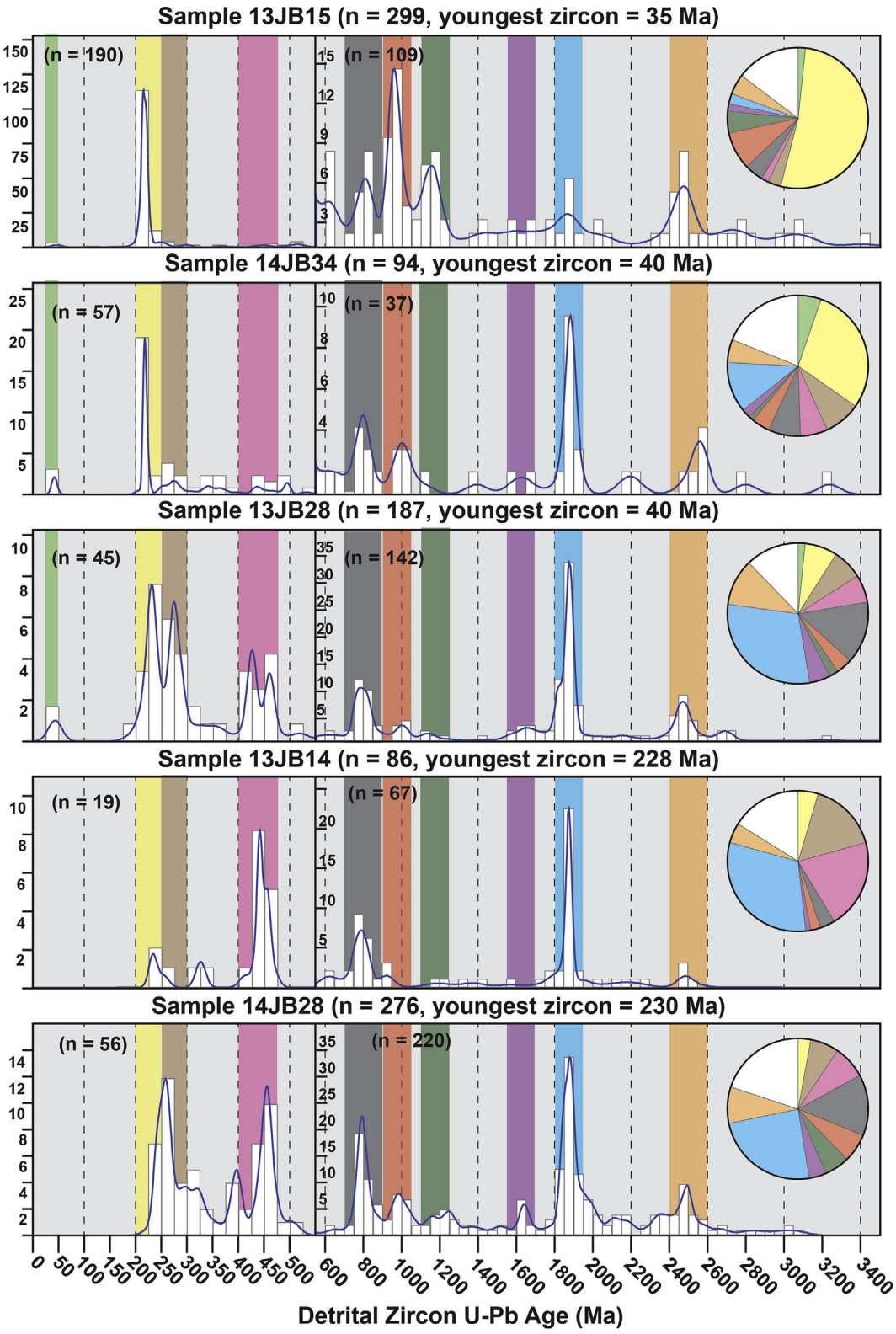

Fig. 6. Detrital zircon U–Pb geochronology results from the nonmarine strata in the Ganzi-Litang suture. Data presented as histogram with comparison of zircon age and frequency, as well as a kernel density estimation curve (blue line). A scale break at 550 Ma is present for visual enhancement of Phanerozoic data. Pie charts illustrate the percent abundance of prominent age populations, which correspond to the vertical color bars. Light green (35–50 Ma), yellow (200–250 Ma), brown (250–300 Ma), pink (400–475 Ma), gray (700–900 Ma), orange (900–105 Ma), dark green (1100–1250 Ma), purple (1550–1700 Ma), blue (1800–1950 Ma), and light brown (2400–2600 Ma). Samples are positioned in relative stratigraphic order.

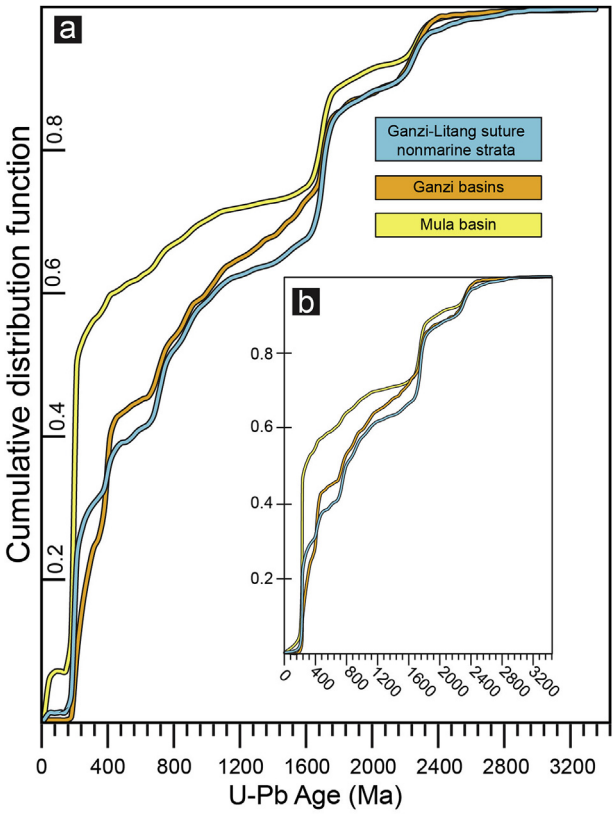

Fig. 7. Cumulative distribution curves comparing geochronology results of nonmarine strata from the Ganzi-Litang suture (blue line; this study), the Mula Basin (yellow line; Jackson et al., 2018a), and the west and east Ganzi basins (orange line; Jackson et al., 2018b). Insert compares same data sets but with all grains less than 200 Ma excluded from cumulative distribution curves, thereby allowing for a comparison without Cenozoic input.

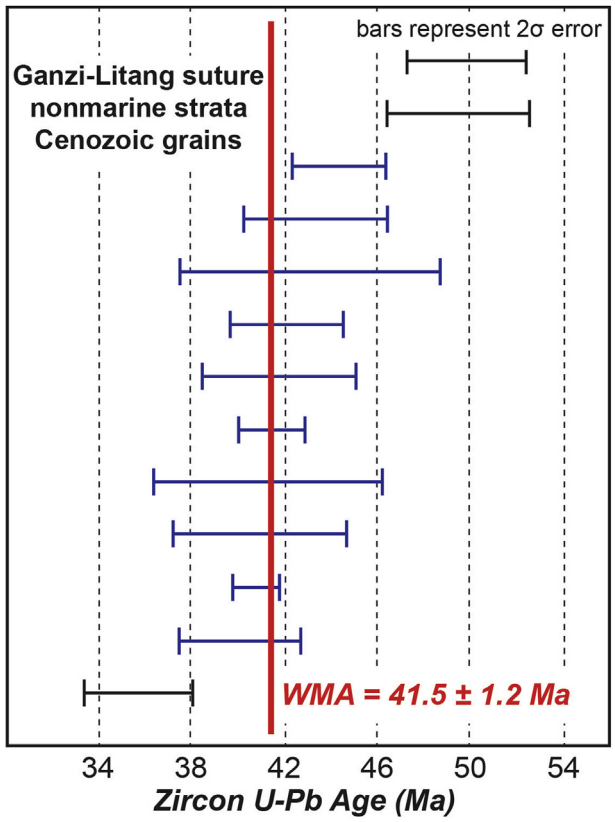

Fig. 8. Weighted mean average of Cenozoic grains from nonmarine strata in the Ganzi-Litang suture. Grain analyses that were incorporated in calculation are blue, while excluded grains are black. The weighted mean average of 41.5 ± 1.2 Ma provides a maximum depositional age for nonmarine strata and an upper-limit for the age of reactivation along the Ganzi-Litang suture.

stratigraphic-geographic proximity and produce similar zircon U–Pb geochronology results, we combined all grains <50 Ma into a single weighted mean average to establish a more robust maximum depositional age (MDA). The calculated weighted mean average for the nonmarine Ganzi-Litang suture strata is 41.5 ± 1.2 Ma (Fig. 8). Because a MDA establishes the maximum age (upper-limit) for a stratigraphic interval, we interpret the undeformed Neogene strata in the Ganzi-Litang suture to establish the minimum age (lower-limit) for nonmarine strata. Using these interpretations, the nonmarine strata in the Ganzi-Litang suture are bracketed in age of ca. 42–25 Ma.

5. Discussion

5.1. Timing and location of deformation and deposition

Apatite (U–Th)/He, zircon fission-track (AFT), and zircon (U–Th)/He results from the Late Triassic Daocheng Pluton, located about 25–30 km southwest of the study area, yield two phases of rapid cooling in the Late Jurassic–Early Cretaceous and Late Oligocene–Early Miocene (Clark et al., 2005a; Tian et al., 2014). Rapid cooling signatures can be used to approximate exhumation responses to either erosion of overburden material, faulting, or a combination of both (e.g., Reiners and Brandon, 2006). The Mula Basin, which consists of nonmarine strata similar to the fault-bounded nonmarine strata in the Ganzi-Litang suture, is in nonconformable contact with the Daocheng Pluton and bound by a reverse fault along its eastern boundary. Jackson et al. (2018a) determined a MDA of 45.5 ± 0.5 Ma for the nonmarine Mula Basin strata, similar our MDA of 41.5 ± 1.2 Ma for nonmarine strata in the Ganzi-Litang suture. Because MDA calculations and the true depositional age of clastic strata contain an inherent lag-time, with the amount of time between the two dependent on numerous transport and depositional parameters, and because of the undeformed Neogene strata present in the Ganzi-Litang suture, we interpret our age determinations for nomarine strata to correlate well to the Late Oligocene–Early Miocene rapid cooling phase. Thereby, nonmarine deposition in the Ganzi-Litang suture and Mula Basin region, along with a rapid Cenozoic cooling signature from thermochronometers seem to record deformation in the southern Yidun terrane. Presumably this deformation represents an upper-crustal response in the eastern Tibetan Plateau to the India-Asia collision.

In contrast to the southern Yidun terrane, nonmarine strata in the west and east Ganzi basins, northern Yidun terrane, yield MDAs of ~215 Ma (Jackson et al., 2018b). The west and east Ganzi basins are both bound by reverse faults that place Late Triassic Yidun Group turbidite rock on top of nonmarine strata and nonconformably overlie the Late Triassic Ganzi Pluton. Jackson et al. (2018b) interpreted the west and east Ganzi basins to be Mesozoic in age and more closely related to the Late Jurassic–Early Cretaceous cooling phase, which presumably is tectonically associated with the Lhasa-Qiangtang collision (e.g., Kapp et al., 2005). Therefore, we suggest two phases of nonmarine deposition that can be distinguished both spatially (northern and southern Yidun terrane) and temporally (Mesozoic and Cenozoic).

Both phases of nonmarine deposition can be associated with structural reactivation episodes along the Ganzi-Litang suture and indicate a contractional deformation regime. Reconstructions of the paleogeographic location of the eastern Tibetan Plateau show that crustal material between the Eastern Himalayan Syntaxis and the Xianshuihe fault zone have been shortened, rotated, and translated to the southeast (Burchfiel et al., 1995; Burchfiel and Chen, 2012). However, it is unlikely that the paleogeographic extent of the northern and southern Yidun terrane were

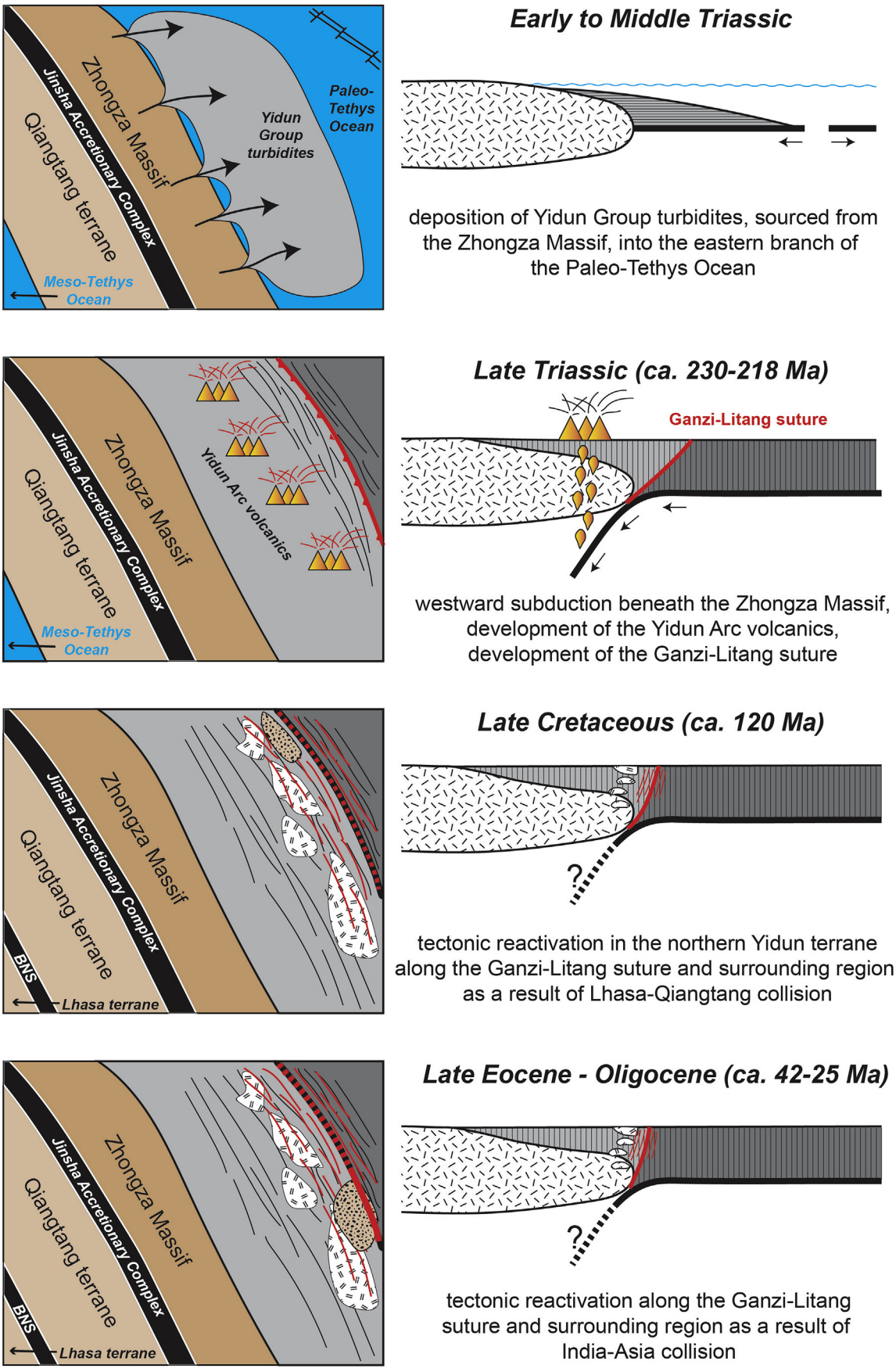

Fig. 9. Interpreted tectonic development of the Ganzi-Litang suture. Red lines represent active faulting, while black lines represent nonactive faults.

substantially displaced with regard to their present day location. We envision the difference in spatial deformation to be a product of different convergent directions (i.e., sigma-one) during collision with respect of the Ganzi-Litang suture. Another explanation may involve differences in crustal rheology along strike in the Ganzi-Litang suture. Wang et al. (2013) documented a difference in the spectrum of detrital U–Pb geochronology ages in Late Triassic turbidie rock (Yidun Group) from the northern and southern parts of the Yidun terrane and inferred a diachronous development of the suture zone. Sun et al. (2018) used analogue models to evaluate the influence of inherited crustal zones of weaknesses on the style and distribution of Cenozoic deformation in the eastern Tibetan Plateau during India-Asia collision. Their best model requires rheology differences between the northern (strong) and southern (weak) Songpan-Ganzi terrane basement. The two contrasting rheological basements of the Songpan-Ganzi are juxtaposed next to the Ganzi-Litang suture and match spatial differences between northern and southern nonmarine strata. These findings seem to indicate that the Ganzi-Litang suture genetically developed differently from south to north and provide motivation for further research along the suture zone.

5.2. Tectonic implications

Rigid block models (e.g., Tapponnier et al., 2001) suggest that suture zones represent lithospheric zones of weaknesses that focus deformation throughout multiple episodes of terrane collisions along the southern margin of Eurasia; predicting that the timing of reactivation along the interior plateau's Mesozoic sutures illustrate the spatial representation of high topography associated with plateau development. In contrast, middle to lower crustal flow models predict decoupling of the crust, where the upper portion passively deforms above a thickened ductile layer (e.g., Clark et al., 2005b). While a hybrid models incorporating these end-member explanations is becoming more common, future models must address the spatial-temporal development of Cenozoic deformation in the eastern and southeastern Tibetan Plateau regions. Specifically, the spatial resolution and amount of Cenozoic contractional deformation in the eastern Tibetan Plateau, prior to the transition to a prevailing strike-slip regime is needed to assess models.

By integrating our results with other structural and geochronological studies, we summarize the tectonic development of the Ganzi-Litang suture from Triassic to Micoene time (Fig. 9). Prior to the initial development of the Ganzi-Litang suture, the Zhongza Massif separated from the Kunlun terrane leaving behind the eastern branch of the Paleo-Tethys Ocean upon which turbidites were deposited (Pullen et al., 2008; Jian et al., 2019). During Late Triassic time (ca. 215–230 Ma) westward subduction of the eastern Paleo-Tethys Ocean, along the north and east part of the Zhongza Massif margin initiated, resulting in the development of the Ganzi-Litang suture and emplacement of Yidun Arc plutons. Subsequent Lhasa amalgamation to the Qiantang terrane in Early–Middle Cretaceous time, resulted in the reactivation, steepening in dip angle, and exhumation of the Ganzi-Litang suture (e.g., Jackson et al., 2018b). The Cenozoic India-Asia collision (ca. 55 Ma; Hu et al., 2016) resulted in another phase of structural reactivation along the Ganzi-Litang suture. This phase of reactivation is recorded in the upper-crustal, contractional deformation and nonmarine deposition in the Ganzi-Litang suture (this study) and the Mula Basin (Jackson et al., 2018b). Our results bracket the timing of reactivation to ca. 45–25 Ma. Temporally, our results allow for enhanced resolution for determining the onset of strike-slip faulting in the region, which is generally assigned a Miocene age (e.g., Zhang et al., 2015).

6. Conclusions

Growth of the Tibetan Plateau, in response to the India-Asia collision, reactivated the Late Triassic Ganzi-Litang suture near Litang during the Cenozoic. Fault-bound synorogenic nonmarine strata in the Ganzi-Litang suture record deformation and deposition associated with reactivation. These spatial-temporal controls for Cenozoic deformation and deposition provide enhanced parameters for assessing tectonic models of the eastern Tibetan Plateau. The following conclusions are made from this study:

(1) The structural juxtaposition of mélange rock and Triassic turbidite rock with respect to nonmarine strata, measured fault plane orientations, and fracture measurements indicate that nonmarine strata are bound by reverse faults along the western and eastern flanks of the Ganzi-Litang suture.
(2) Conglomerate clast counts show that nonmarine strata were sourced locally from Triassic Yidun Group turbidites, Late Triassic Yidun Arc plutons, and Ganzi-Litang suture rock. Detrital zircon age determinations show grain populations at 200–250 Ma, 250–300 Ma, 400–480 Ma, 720–880 Ma, 900–1000 Ma, ~1800 Ma, and ~2450 Ma, suggesting a relatively small, drainage network that incorporated Triassic Yidun Group turbidite and Triassic Yidun Arc pluton rocks.
(3) Weighted mean average of Cenozoic zircon grains from synorogenic nonmarine strata in the Ganzi-Litang suture. Results indicate a maximum depositional age for nonmarine strata of 41.5 ± 1.2 Ma. This maximum depositional age establishes the upper-limit for Cenozoic reactivation along the Ganzi-Litang suture, while the undeformed Neogene strata in the Ganzi-Litang suture establish a lower-limit. Therefore, we suggest a Late Eocene–Oligocene age (ca. 42–25 Ma) for reactivation.

Acknowledgements

This work was supported by U.S. National Science Foundation grants EAR-1119266 (Robinson) and EAR-1119219 (Weislogel). The University of Alabama Graduate School and Department of Geological Sciences provided travel support. The authors wish to thank Chunmiao Zheng (South University of Science and Technology of China) and Fei Shang (China Petroleum Corporation) for assistance with permits and fieldwork. Zircon analyses were conducted at the University of Arizona's LaserChron Center (EAR-1338583). Comments by two anonymous reviewers greatly improved this work.

Appendix A. Supplementary data

Supplementary data to this article can be found online at https://doi.org/10.1016/j.gsf.2019.11.001.

References

Black, L.P., Kamo, S.L., Allen, C.M., Davis, D.W., Aleinikoff, J.N., Valley, J.W., Mundil, R., Campbell, I.H., Korsch, R.J., Williams, I.S., Foudoulis, C., 2004. Improved $^{206}Pb/^{238}U$ microprobe geochronology by the monitoring of a trace-element-related matrix effect; SHRIMP, ID-TIMS, ELA-ICP-MS and oxygen isotope documentation for a series of zircon standards. Chem. Geol. 205, 115–140. https://doi.org/10.1016/j.chemgeo.2004.01.003.

Burchfiel, B.C., Chen, Z., Liu, Y., Royden, L.H., 1995. Tectonics of the Longmen Shan and adjacent regions. Int. Geol. Rev. 37, 661–735. https://doi.org/10.1080/00206819509465424.

Burchfiel, B.C., Chen, Z.L., 2012. Tectonics of the southeastern Tibetan Plateau and its adjacent foreland. Geol. Soc. Am. Mem. 210, 231.

Chevalier, M., Leloup, P., Replumaz, A., Pan, J., Liu, D., Li, H., Gourbet, L., Metois, M., 2016. Tectonic-geomorphology of the Litang fault system, SE Tibetan Plateau, and implication for regional seismic hazard. Tectonophysics 682, 278–292. https://doi.org/10.1016/j.tecto.2016.05.039.

Chung, S.-L., Chu, M.-F., Zhang, Y., Xie, Y., Lo, C.-H., Lee, T.-Y., Lan, C.-Y., Li, X., Zhang, Q., Wang, Y., 2005. Tibetan tectonic evolution inferred from spatial and temporal variations in post-collisional magmatism. Earth Sci. Rev. 68, 173–196. https://doi.org/10.1016/j.earscirev.2004.05.001.

Clark, M.K., House, M.A., Royden, L.H., Whipple, K.X., Burchfiel, B.C., Zhang, X., Tang, W., 2005a. Late Cenozoic uplift of southeastern Tibet. Geology 33 (6), 525–528. https://doi.org/10.1130/G21265.1.

Clark, M.K., Bush, J.W.M., Royden, L.H., 2005b. Dynamic topography produced by lower crustal flow against rheological strength heterogeneities bordering the Tibetan Plateau. Geophys. J. Int. 162, 575–590. https://doi.org/10.1111/j.1365-246X.2005.02580.x.

Daly, M.C., Chorowicz, J., Fairhead, J.D., 1989. Rift basin evolution of Africa: the influence of reactivated steep basement shear zones. In: Cooper, M.A., Williams, G.D. (Eds.), Inversion Tectonics, vol. 44. Geological Society of London Special Publication, pp. 309–334.

DeCelles, P.G., Carrapa, B., Gehrels, G.E., 2007a. Detrital zircon U-Pb ages provide provenance and chronostratigraphic information from Eocene synorogenic deposits in northwestern Argentina. Geology 35 (4), 323–326. https://doi.org/10.1130/G23322A.1.

DeCelles, P.G., Kapp, P., Ding, L., Gehrels, G.E., 2007b. Late Cretaceous to middle Tertiary basin evolution in the central Tibetan Plateau: changing environments in response to tectonic partitioning, aridification, and regional elevation gain. Geol. Soc. Am. Bull. 119, 654–680. https://doi.org/10.1130/B26074.1.

Dewey, J.F., 1977. Suture zone complexities: a review. Tectonophysics 40 (1–2), 53–67. https://doi.org/10.1016/0040-1951(77)90029-4.

Dewey, J.F., Burke, K.C.A., 1973. Tibetan, Variscan, and Precambrian basement reactivation: products of continental collision. J. Geol. 81 (6), 683–692. https://doi.org/10.1086/627920.

Dewey, J.F., Shackleton, R.M., Chengfa, C., Yiyin, S., 1988. The tectonic evolution of the Tibetan Plateau. Philos. Trans. R. Soc. Lond. 327, 379–413.

Ding, L., Yang, D., Cai, F.L., Pullen, A., Kapp, P., Gehrels, G.E., Zhang, L.Y., Zhang, Q.H., Lai, Q.Z., Yue, Y.H., Shi, R.D., 2013. Provenance analysis of the mesozoic Hoh-Xil-Songpan-Ganzi turbidites in northern Tibet: implications for the tectonic evolution of the eastern Paleo-Tethys Ocean. Tectonics 32 (1), 34–48. https://doi.org/10.1002/tect.20013.

Engelder, T., 1987. Joints and shear fractures in rock. Fract. Mech. Rock X, 27–69.

Gehrels, G.E., Valencia, V., Ruiz, J., 2008. Enhanced precision, accuracy, efficiency, and spatial resolution of U-Pb ages by laser ablation-multicollector-inductively coupled plasma-mass spectrometry. Geochem. Geophys. Geosyst. 9, Q03017. https://doi.org/10.1029/2007GC001805.

Gehrels, G., Pecha, M., 2014. Detrital zircon U-Pb geochronology and Hf isotope geochemistry of Paleozoic and Triassic passive margin strata of western North America. Geosphere 10 (1), 49–65. https://doi.org/10.1130/GES00889.1.

Holdsworth, R.E., Butler, C.A., Roberts, A.M., 1997. The recognition of reactivation during continental deformation. J. Geol. Soc. Lond. 154, 73–78.

Holdsworth, R.E., Stewart, M., Imber, J., Strachan, R.A., 2001. The structure and rheological evolution of reactivated continental fault zones: a review and case study. In: Miller, J.A., Holdsworth, R.E., Buick, I.S., Hand, M. (Eds.), Continental Reactivation and Reworking, vol. 184. Geological Society of London Special Publication, pp. 115–137.

Horton, B.K., Yin, A., Spurlin, M.S., Zhou, J., Wang, J., 2002. Paleocene-Eocene syncontractional sedimentation in narrow, lacustrine-dominated basins of east-central Tibet. Geol. Soc. Am. Bull. 114, 771–786. https://doi.org/10.1130/0016-7606(2002)114<0771.

Horton, B.K., Dupont-Nivet, G., Zhou, J., Waanders, G.L., Butler, R.F., Wang, J., 2004. Mesozoic-Cenozoic evolution of the Xining-Minhe and Dangchang basins, northeastern Tibetan Plateau: magnetostratigraphic and biostratigraphic results. J. Geophys. Res. 109, B04402. https://doi.org/10.1029/2003JB002913.

Hou, Z., 1993. Tectonic–magmatic evolution of the Yidun island-arc and geodynamic setting of kuroko-type sulfide deposits in Sanjiang region, SW China. In: Ishihara, S., Urabe, T., Ohmoto, H. (Eds.), Mineral Resources Symposia; Volume C. Selected Papers from the Symposia I-3-47, II-16-5, II-16-10 and II-16-12, Ferro-Manganese Deposits, Anoxic Sediments and Massive Sulfide Deposits. Shigen Chishitsu Special Issue 17. Society of Resource Geologists of Japan, Tokyo, Japan, pp. 336–350.

Hu, X., Garzanti, E., Wang, J., Huang, W., An, W., Webb, A., 2016. The timing of India-Asia collision onset – Facts, theories, controversies. Earth Sci. Rev. 160, 264–299. https://doi.org/10.1016/j.earscirev.2016.07.014.

Jackson Jr., W.T., Robinson, D.M., Weislogel, A.L., Jian, X., McKay, M.P., 2018a. Cenozoic development of the nonmarine Mula basin in the southern Yidun terrane: deposition and deformation in the eastern Tibetan Plateau associated with the India-Asia collision. Tectonics 37, 2446–2465. https://doi.org/10.1029/2018TC004994.

Jackson Jr., W.T., Robinson, D.M., Weislogel, A.L., Shang, F., Jian, X., 2018b. Mesozoic development of nonmarine basins in the northern Yidun terrane: deposition and deformation in the eastern Tibetan Plateau prior to the Inidia-Asia collision. Tectonics 37, 2466–2485. https://doi.org/10.1029/2018TC004995.

Jian, X., Weislogel, A., Pullen, A., 2019. Triassic sedimentary filling and closure of the eastern Paleo-Tethys Ocean: new insights from detrital zircon geochronology of Songpan-Ganzi, Yidun and west Qinling flysch in eastern Tibet. Tectonics. https://doi.org/10.1029/2018TC005300.

Kapp, P., Yin, A., Harrison, T.M., Ding, L., 2005. Cretaceous-Tertiary shortening, basin development, and volcanism in central Tibet. Geol. Soc. Am. Bull. 117, 865–878. https://doi.org/10.1130/B25595.1.

Kapp, P., DeCelles, P.G., Gehrels, G.E., Heizler, M., Ding, L., 2007. Geological records of the Lhasa-Qiangtang and Indo-Asian collisions in the Nima area of central Tibet. Geol. Soc. Am. Bull. 119, 917–932. https://doi.org/10.1130/B26033.1.

Kroner, A., Greiling, R., Reischmann, T., Hussein, I.R.M., Stern, R.J., Durr, S., Kruger, J., Zimmer, M., 1987. Pan-African crustal evolution in the Nubian segment of northeast Africa. In: Kroner, A. (Ed.), Proterozoic Lithopshere Evolution, vol. 17. American Geophysical Union Geodynamics Series, pp. 235–257.

Leary, R.J., DeCelles, P.G., Quade, J., Gehrels, G.E., Waanders, G., 2016. The Liuqu Conglomerate, southern Tibet: early Miocene basin development related to deformation within the Great Counter Thrust system. Lithosphere 8, 427–450. https://doi.org/10.1130/L542.1.

Leier, A.L., DeCelles, P.G., Kapp, P., Ding, L., 2007a. The Takena Formation of the Lhasa terrane, southern Tibet: the record of a Late Cretaceous retroarc foreland basin. Geol. Soc. Am. Bull. 119, 31–48. https://doi.org/10.1130/B25974.1.

Leier, A.L., Kapp, P., Gehrels, G.E., DeCelles, P.G., 2007b. Detrital zircon geochronology of Carboniferous-Cretaceous strata in the Lhasa terrane, southern Tibet. Basin Res. 19, 361–378. https://doi.org/10.1111/j.1365-2117.2007.00330.x.

LeLoup, P.H., Lacassin, R., Tapponnier, P., Scharer, U., Zhong, D., Liu, X., Zhang, L., Ji, S., Trinh, P.T., 1995. The Ailao Shan-Red River shear zone (Yunnan, China), Tertiary transform boundary of Indochina. Tectonophysics 251, 13–84.

Leng, C.B., Huang, Q.Y., Zhang, X.C., Wang, S.X., Zhong, H., Hu, R.Z., Bi, X.W., Zhu, J.J., Wang, X.S., 2014. Petrogenesis of the late Triassic volcanic rocks in the southern Yidun Arc, SW China: constraints from the geochronology, geochemistry, and Sr-Nd-Pb-Hf isotopes. Lithos 190/191, 363–382. https://doi.org/10.1016/j.lithos.2013.12.018.

Li, Q.-H., Zhang, Y., Zhang, K., Yan, L., Zeng, L., Jin, Z., Sun, J., Zhou, X., Tang, X., Lu, L., 2017. Garnet amphibolites from the Ganzi-Litang fault zone, eastern Tibetan Plateau: mineralogy, geochemistry, and implications for evolution of the eastern Palaeo-Tethys Realm. Int. Geol. Rev. 60 (16), 1954–1967. https://doi.org/10.1080/00206814.2017.1396563.

Ludwig, K.R., 2012. A Geochronological Toolkit for Microsoft Excel, vol. 5. Berkeley Geochronology Center Special Publication, p. 75.

Marshak, S., Karlstrom, K., Timmons, J.M., 2000. Inversion of Proterozoic extensional faults: an explanation for the pattern of Laramide and Ancestral Rockies intracatonic deformation, United States. Geology 28, 735–738. https://doi.org/10.1130/0091-7613(2000)28<735:IOPEFA>2.0.CO;2.

Molnar, P., 1989. The geologic evolution of the Tibetan Plateau. Am. Sci. 77 (4), 350–360.

Orme, D.A., Carrapa, B., Kapp, P., 2015. Sedimentology, provenance and geochronology of the upper Cretaceous-lower Eocene western Xigaze forearc basin, southern Tibet. Basin Res. 27, 387–411. https://doi.org/10.1111/bre.12080.

Peng, T., Zhao, G., Fan, W., Peng, B., Mao, Y., 2014. Zircon geochronology and Hf isotopes of Mesozoic intrusive rocks from the Yidun terrane, Eastern Tibetan Plateau: petrogenesis and their bearings with Cu mineralization. J. Asian Earth Sci. 80, 18–33. https://doi.org/10.1016/j.jseaes.2013.10.028.

Pullen, A., Kapp, P., Chang, H., McCallister, A.T., Garzione, C.N., Gehrels, G.E., Heermance, R.V., Ding, L., 2011. The Qaidam Basin and northern Tibetan Plateau as dust sources for the Chinese Loess Plateau, determined by U-Pb detrital zircon provenance. Geology 39 (11), 1031–1034. https://doi.org/10.1130/G32296.1.

Pullen, A., Kapp, P., Gehrels, G., Vervoort, J., Ding, L., 2008. Triassic continental subduction in central Tibet and Mediterranean-style closure of the Paleo-Tethys Ocean. Geology 36 (5), 351–354. https://doi.org/10.1130/G24435A.1.

Reid, A.J., Wilson, C.J.L., Liu, S., 2005. Structural evidence for the permo-Triassic tectonic evolution of the Yidun Arc, eastern Tibetan plateau. J. Struct. Geol. 27 (1), 119–137. https://doi.org/10.1016/j.jsg.2004.06.011.

Reid, A.J., Wilson, C.J.L., Liu, S., Pearson, N., Belousova, E., 2007. Mesozoic plutons of the Yidun Arc, SW China: U/Pb geochronology and Hf isotopic signature. Ore Geol. Rev. 31, 88–106. https://doi.org/10.1016/j.oregeorev.2004.11.003.

Reiners, P.W., Brandon, M.T., 2006. Using thermochronology to understand orogenic erosion. Annu. Rev. Earth Planet Sci. 34, 419–466.

Ridgway, K.D., Trop, J.M., Nokleberg, W.J., Davidson, C.M., Eastham, K.R., 2002. Mesozoic and Cenozoic tectonics of the eastern and central Alaska Range: progressive basin development and deformation in a suture zone. Geol. Soc. Am. Bull. 114 (12), 1480–1504.

Roger, F., Tapponnier, P., Arnaud, N., Scharer, U., Brunel, M., Zhiqin, X., Jingsui, Y., 2000. An Eocene magmatic belt across central Tibet: mantle subduction triggered by the Indian collision? Terra Nova 12, 102–108. https://doi.org/10.1046/j.1365-3121.2000.123282.x.

Royden, L.H., Burchfiel, B.C., van der Hilst, R.D., 2008. The geological evolution of the Tibetan Plateau. Science 321, 1054–1058. https://doi.org/10.1126/science.1155371.

Spurlin, M.S., Yin, A., Horton, B.K., Zhou, J., Wang, J., 2005. Structural evolution of the Yushu-Nangqian region and its relationship to syn-collisional igneous activity, east-central Tibet. Geol. Soc. Am. Bull. 117, 1293–1317. https://doi.org/10.1130/B25572.1.

Staisch, L.M., Niemi, N.A., Hong, C., Clark, M.K., Rowley, D.B., Currie, B., 2014. A Cretaceous-Eocene depositional age for the Fenghuoshan Group, Hoh Xil Basin: implications for the tectonic evolution of the northern Tibet Plateau. Tectonics 33, 281–301. https://doi.org/10.1002/2013TC003367.

Studnicki-Gizbert, C., Burchfiel, B.C., Li, Z., Chen, Z., 2008. Early Tertiary Gonjo basin, eastern Tibet: sedimentary and structural record of the early history of India-Asia collision. Geosphere 4, 713–735. https://doi.org/10.1130/GES00136.1.

Sun, M., Yin, A., Yan, D., Ren, H., Mu, H., Zhu, L., Qiu, L., 2018. Role of pre-exisiting structures in controlling the Cenozoic tectonic evolution of the eastern Tibetan Plateau: new insights from analogue experiments. Earth Planet. Sci. Lett. 491, 207–215. https://doi.org/10.1016/j.epsl.2018.03.005.

Tapponnier, P., Zhiqin, X., Roger, F., Meyer, B., Arnaud, N., Wittlinger, G., Jingsui, Y., 2001. Oblique stepwise rise and growth of the Tibet Plateau. Science 294, 1671–1677. https://doi.org/10.1126/science.105978.

Tian, Y., Kohn, B.P., Gleadow, A.J.W., Hu, S., 2014. A thermochronological perspective on the morphotectonic evolution of the southeastern Tibetan Plateau. J. Geophys. Res.: Solid Earth 119, 676–698. https://doi.org/10.1002/2013JB010429.

Thatcher, W., 1995. Microplate verse continuum descriptions of active tectonic deformation. J. Geophys. Res.: Solid Earth 100, 3885–3894.

Thomas, W.A., 1977. Evolution of Appalachian-Ouachita salients and recesses from reentrants and promontories in the continental margin. Am. J. Sci. 277, 1233–1278. https://doi.org/10.2475/ajs.277.10.1233.

Vermeesch, P., 2012. On the visualization of detrital age distributions. Chem. Geol. 312–313, 190–194. https://doi.org/10.1016/j.chemgeo.2012.04.021.

Wang, B.Q., Wang, W., Chen, W.T., Gao, J.F., Zhao, X.F., Yan, D.P., Zhou, M.F., 2013. Constraints of detrital zircon U-Pb ages and Hf isotopes on the provenance of the Triassic Yidun Group and tectonic evolution of the Yidun Terrane, Eastern Tibet. Sediment. Geol. 289, 74–98. https://doi.org/10.1016/j.sedgeo.2013.02.005.

Wang, Q., Wyman, D.A., Xu, J., Dong, Y., Vasconcelos, P.M., Pearson, N., Wan, Y., Dong, H., Li, C., Yu, Y., Zhu, T., Feng, X., Zhang, Q., Zi, F., Chu, Z., 2008a. Eocene melting of subducting continental crust and early uplifting of central Tibet: evidence from central-western Qiangtang high-K calc-alkaline andesites, dacites and rhyolites. Earth Planet. Sci. Lett. 272 (1–2), 158–171. https://doi.org/10.1016/j.epsl.2008.04.034.

Wang, C., Zhao, X., Liu, Z., Lippert, P.C., Graham, S.A., Coe, R.S., Yi, H., Zhu, L., Liu, S., Li, Y., 2008b. Constraints on the early uplift history of the Tibetan Plateau. Proc. Natl. Acad. Sci. 105 (13), 4987–4992. https://doi.org/10.1073/pnas.0703595105.

Wang, E., Burchfiel, B.C., 1997. Interpretation of Cenozoic tectonics in the right-lateral accommodation zone between the Ailao Shan shear zone and the eastern Himalayan syntaxis. Int. Geol. Rev. 39, 191–219. https://doi.org/10.1080/00206819709465267.

Wang, E., Burchfiel, B.C., 2000. Late Cenozoic to Holocene deformation in southwest Sichuan and adjacent Yunnan, China, and its role in formation of the southeastern part of the Tibetan Plateau. Geol. Soc. Am. Bull. 112, 413–423. https://doi.org/10.1130/0016-7606(2000)112<413:LCTHDI>2.0.CO;2.

Weislogel, A.L., Graham, S.A., Chang, E.Z., Wooden, J.L., Gehrels, G.E., Yang, H., 2006. Detrital zircon provenance of the late Triassic Songpan-Ganzi complex: sedimentary record of collision of the north and south China blocks. Geology 34, 97–100. https://doi.org/10.1130/G21929.

Weislogel, A.L., 2008. Tectonostratigraphic and geochronologic constraints on evolution of the northeast paleotethys from the Songpan-Ganzi complex, Central China. Tectonophysics 451 (1–4), 331–345. https://doi.org/10.1016/j.tecto.2007.11.053.

Weislogel, A.L., Graham, S.A., Chang, E.Z., Wooden, J.L., Gehrels, G.E., 2010. Detrital zircon provenance from three turbidite depocenters of the middle-upper Triassic Songpan-Ganzi complex, Central China: record of collisional tectonics, erosional exhumation, and sediment production. Geol. Soc. Am. Bull. 122 (11/12), 2041–2062. https://doi.org/10.1130/B26606.1.

Xia, L., Li, X., Ma, Z., Xu, X., Xia, Z., 2011. Cenozoic volcanism and tectonic evolution of the Tibetan plateau. Gondwana Res. 19, 850–866. https://doi.org/10.1016/j.gr.2010.09.005.

Yang, T.N., Hou, Z.Q., Wang, Y., Zhang, H.R., Wang, Z.L., 2012. Late Paleozoic to Early Mesozoic tectonic evolution of northeast Tibet: evidence from the Triassic composite western Jinsha-Garze-Litang suture. Tectonics 31, TC4004. https://doi.org/10.1029/2011TC003044.

Yin, A., Harrison, T.M., 2000. Geologic evolution of the Himalayan–Tibetan Orogeny. Annu. Rev. Earth Planet Sci. 28, 211–280.

Zhang, K., Zhang, Y., Tang, X., Xia, B., 2012. Late Mesozoic tectonic evolution and growth of the Tibetan Plateau prior to the Indo-Asian collision. Earth Sci. Rev. 114 (3–4), 236–249. https://doi.org/10.1016/j.earscirev.2012.06.001.

Zhang, Y.Z., Replumaz, A., Wang, G.C., Leloup, P.H., Gautheron, C., Bernet, M., van der Beek, P., Paquette, J.L., Wang, A., Zhang, K.X., Chevalier, M.L., Li, H.B., 2015. Timing and rate of exhumation along the Litang fault system, implication for fault reorganization in Southeast Tibet. Tectonics 34, 1219–1243. https://doi.org/10.1002/2014TC003671.